16th ICAAR LISBOA 2020-2022

16th International Conference on
Alkali-Aggregate Reaction in Concrete
Lisboa | LNEC | Portugal | 31 May - 2 June 2022

http://icaar2020-2022.lnec.pt

# Characterization of synthetic ASR products by TEM and preliminary comparison with on-field early stage products

**S. Barbotin-Albinski [(1)], Z. Shi [(2)], E. Boehm-Courjault [(1)], A. Leemann [(2)], K. Scrivener [(1)]**

*(1) Laboratory of construction materials, Swiss Federal Institute of Technology EPFL, 1015 Lausanne, Switzerland, solene.barbotin@epfl.ch*

*(2) Laboratory for Concrete & Construction Chemistry, Swiss Federal Laboratories for Materials Science and Technology (Empa), 8600 Dübendorf, Switzerland*

**Abstract**

*The composition and structures of ASR products located in aggregates and cement paste can vary substantially. In a novel approach using SEM, FIB and TEM, early stage products formation can be studied, and comparison with late stage and synthetic products is made possible. Three synthesized ASR products with various alkali content and two field products from different structures in Switzerland have been analysed by STEM to define their morphology, composition and structure. Morphology and structure are linked in synthetic samples: platey products are crystalline corresponding to K- or Na-shlykovite, and fibrillar/globular products are nanocrystalline, corresponding to ASR-P1 and/or eventually C-S-H. In field samples, platey products are weakly crystalline whereas the globular products are amorphous. Finally, synthetic and some field samples are quite similar in terms of morphology and overall composition.*

***Keywords**: alkali-silica reaction; composition; electron microscopy; morphology; structure*

## 1. INTRODUCTION

Alkali-Silica Reaction (ASR) occurring in concrete structures is one of the main issues impairing concrete durability. Metastable silicates present in aggregates are dissolved by hydroxyl ions present in the alkaline pore solution of the concrete. The dissolved silica then bonds mainly to water, calcium and alkali ions resulting in the formation of reaction products, which induce stress in the aggregates and subsequent cracking. A preliminary survey indicates that in Switzerland, more than 400 structures are affected [1].

There is thus a great need to improve our knowledge about ASR formation in order to prevent it. Even though the basics of mechanisms seem to be known, there are still many open questions regarding the role of the environment, the role of the different components, and the ageing behaviour, as well as the mineral phases reactivity. It was difficult to determine if a given aggregate/cement combination is deleteriously expansive due to the very slow nature of reaction in Switzerland's climate before accelerated expansion tests came into use. Swiss aggregates are an issue concerning ASR occurrence as they often contain minerals which are vulnerable to ASR: around 90% of the aggregates were classified as potentially reactive by [2].

Some facts are nowadays confirmed and quite well defined: the chemistry and thermodynamics of the reaction [3,4], the chemical composition of reaction products, which main components are Si, Ca, K and Na [5-13], the fact that ASR is not one product but that it forms several products [7,11,14,15]. So far, ASR products formed at late stage have been analysed once they are present in large quantities in big cracks (> 20 µm). Results about the early stage formation are needed for a better understanding of the mechanism of cracking. The very low amount of product found at early stage makes its analysis difficult, thus increasing interest in comparison between the early stage products and synthetic ASR products from laboratory synthesis produced by Shi [16]. Comparison between samples from concrete structures ("field samples") and synthetic samples opens a possibility of a more in depth and comprehensive characterisation [17], as synthetic samples can be produced in large quantities.

# 2. MATERIALS AND METHODS

## 2.1 SEM analysis and FIB cutting for field samples

### 2.1.1 Samples

Samples were collected in Switzerland on a dam and on a retaining wall at the Brünig pass in Meiringen (Canton Bern), both severely affected by ASR. The dam is a gravity dam built in 1950, at 1850 m of altitude. The Brünig pass wall is about 40 years old, at around 1000 m of altitude. The samples are respectively named Dam and Brünig in this study, and two lamellae were prepared for each : Dam L1, Dam L2, Brünig L1 and Brünig L2. Each region of interest was selected according to the following criteria:

- > 100 µm away from the interface aggregate/cement matrix
- In the outer 2 mm of the aggregate (Fig. 2.1)
- In a crack < 1.5 µm
- In a $SiO_2$ mineral phase

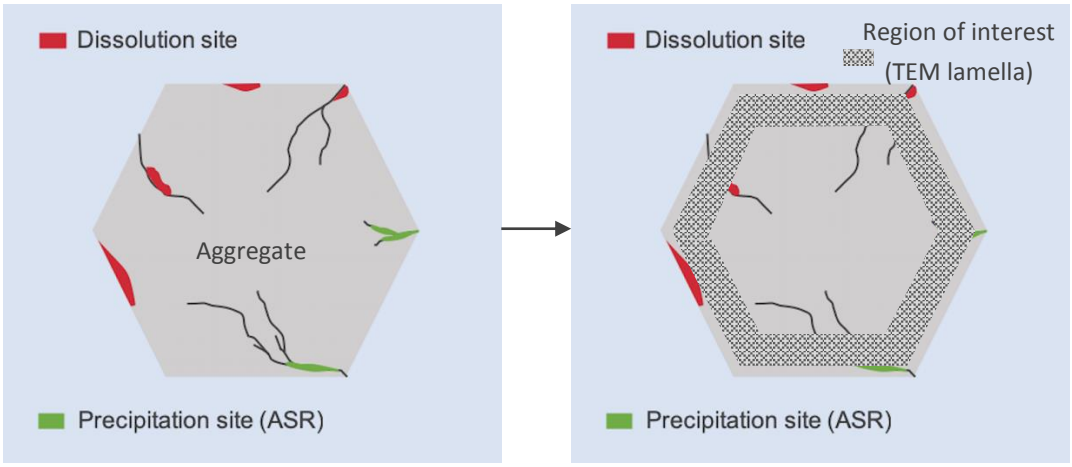


Figure 2.1: Illustration of the region of interest location in an aggregate.

### 2.1.2 Preparation

The regions of interest in the samples were located first by SEM imaging and confirmed by energy-dispersive X-ray spectroscopy (EDX). A line scan across the crack is done and an increase of calcium and alkalis content of a few atomic percent (mostly from 1 to 5 percent) is looked for to confirm the presence of ASR in the thin crack (< 2 µm). Once localized, the region of interest is cut perpendicular to the crack, using a focused ion beam (FIB). Thinning of the lamella (see Figure 2.2) is done at progressively decreasing voltages and currents, ranging from 30kV-27nA down to 5kV-80pA, in order to optimize the time spent and to prevent beam damage. A thin lamella of approximate dimensions 10x12µm and thickness 200nm is obtained and welded to a TEM grid for further analysis regarding composition and structure.

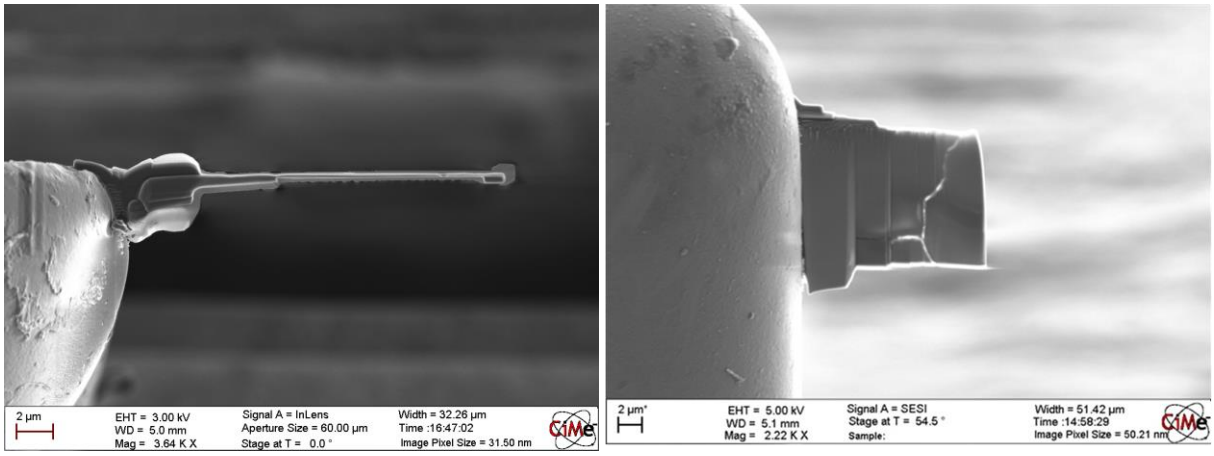


Figure 2.2: TEM lamella after thinning in the FIB top view (left) and side view (right).

## 2.2 TEM grid preparation for synthetic samples

### 2.2.1 Sample

Three different samples termed SNC, $SK_{0.25}N_{0.25}C$ and SKC from [16] are investigated, where the major phases are Na-shlykovite, ASR-P1 and K-shlykovite, respectively, based on powder X-ray diffraction analysis. They were synthesized at a temperature of 80°C. In this paper, they are respectively renamed SNC, SKNC and SKC. The reaction products contained silicon (S), calcium (C), potassium (K) and/or sodium (N) in various quantities, which will be assessed in the results.

### 2.2.2 Preparation

The synthetic powder was dispersed in ethanol, and a drop of the solution is placed on a Holey Carbon film copper grid, 200 mesh, 50 microns, for the STEM analysis. When dried out, the grid is stored under high vacuum.

## 2.3 STEM analysis

The product was studied in STEM mode (scanning TEM mode) to perform EDX measurements. Diffraction patterns have been obtained from specific areas of the sample using selected area electron diffraction (SAED). The parameters used for analysis with STEM are also important to preserve the product, and thus analysis is performed at a rather low voltage, 80kV instead of the usual 200kV, and the cumulative electron dose was kept low, below $5 \times 10^2$ e/Å$^2$, when compared with [18].

For EDX measurements, the sample is tilted by 20° to improve X-rays collection efficiency and a defocus of approximately 200nm is used to avoid beam damage. The analysis is then done after selecting the region of interest.

# 3. RESULTS AND DISCUSSION

## 3.1 Morphology and structure

### 3.1.1 SNC

In SNC sample, ASR products have the following characteristics based on STEM analysis:

- A very well-defined platelet-like or rod-like structure corresponding to Na-shlykovite as seen in Figures 3.1 (left) and 3.2 (left)
- It is crystalline (Figure 3.1 right).
- In dark field, the micro-crystalline behavior of its rods is clearly shown by the brighter areas which show crystallographic planes with the same orientation (Figure 3.2 (left)). Additional features could be observed in Figure 3.2 (right), such as atomic plane alignment, in line with the layered-silicate structure of Na-shlykovite reported in [16].

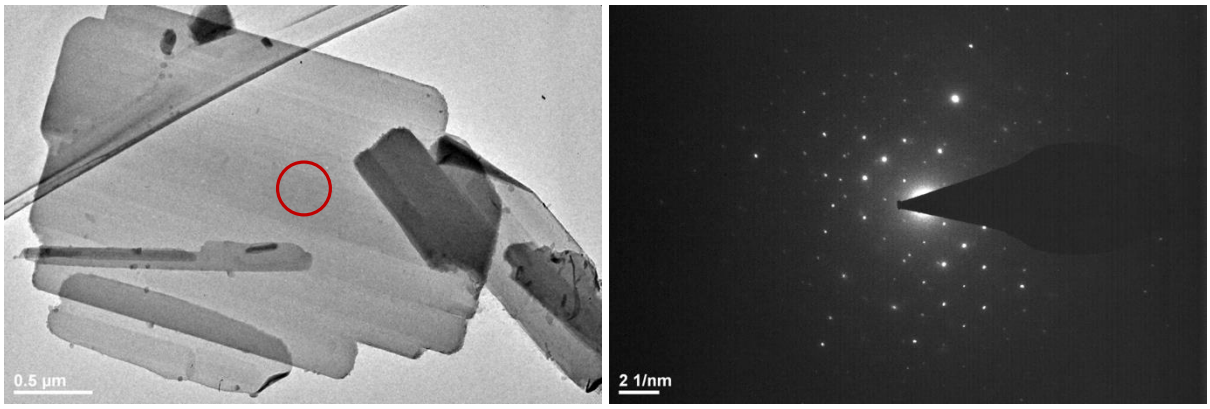


Figure 3.1: Platelet-like Na-shlykovite structure of SNC sample (left) and diffraction pattern from the red zone (right)

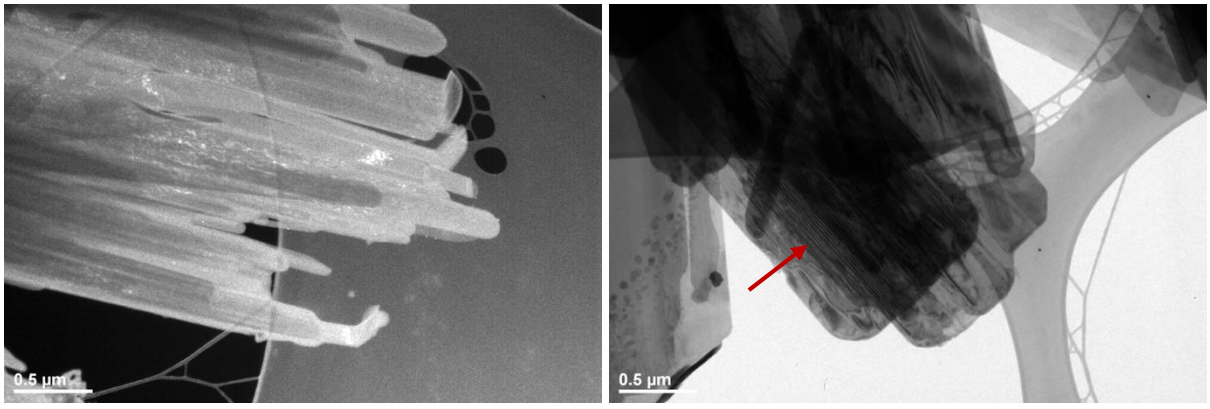


Figure 3.2: Dark field image showing the micro-crystallinity of the Na-shlykovite (left) and bright field image showing atomic planes alignments (right, red arrow)

### 3.1.2 SKC

In SKC sample, ASR products have the following characteristics based on STEM analysis:

- They present different structures. Only one occurrence of platelet-like product (corresponding K-shlykovite) as in Figure 3.3 (right) was found, whereas the rest of the products were found to have a fibrillar structure (likely to be ASR-P1) in Figure 3.5 (left) or a more fluffy (or globular) appearance (likely to be C-S-H) like in Figure 3.3 (right), since K-shlykovite and ASR-P1 can co-precipitate with C-S-H as observed from experiments and also predicted by thermodynamic modelling [19].
- All products are crystalline but at different scales as can be clearly seen in Figure 3.4 and 3.5 (right). The fluffy and fibrillar product (ASR-P1) shows a very interesting nanocrystalline diffraction pattern (Figure 3.4 (right) and 3.5 (right)), whereas the platelet-like product (K-shlykovite) shows a crystalline diffraction pattern with a clear orientation (Figure 3.4 (left)).

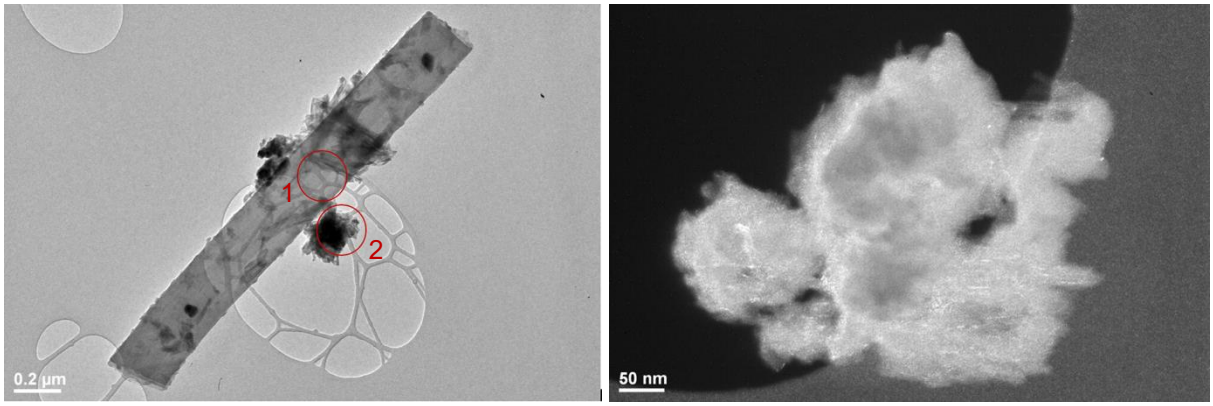


Figure 3.3: Two different products types. Platelet-like K-shlykovite (circle1) and fluffy product (circle2) (left) and dark field image showing the nanocrystalline structure of the SKC ASR globular structure (right).

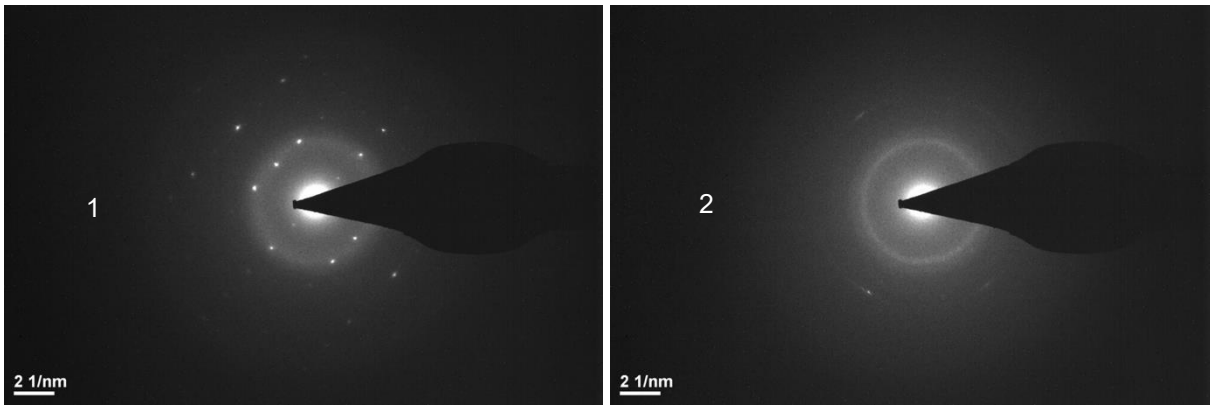


Figure 3.4: Diffraction patterns showing crystallinity of the analyzed area 1 (left) and the weak nano-crystallinity of the analyzed area 2 (right).

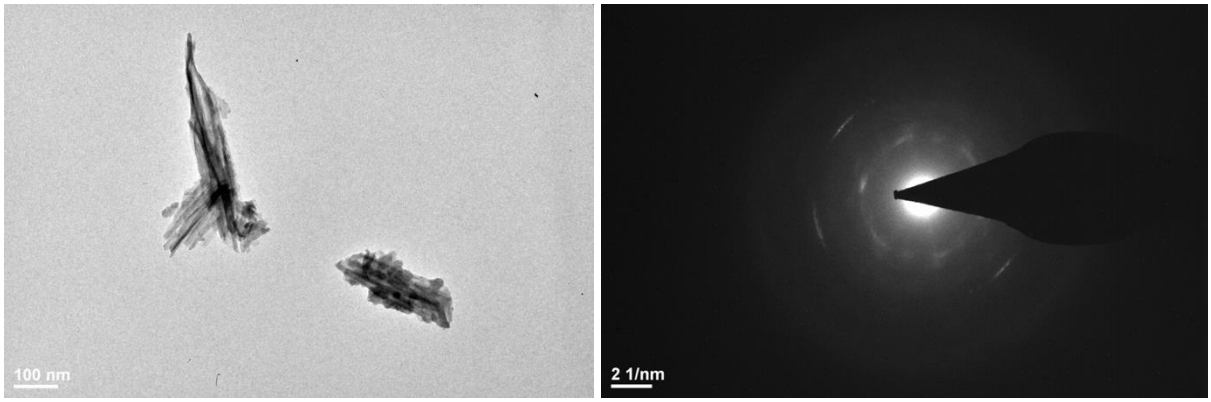


Figure 3.5: Fibrillar product ASR-P1 (left) and corresponding nanocrystalline diffraction pattern (right).

### 3.1.3 SKNC

In SKNC sample, ASR products have the following characteristics based on STEM analysis:

- Most of the observed ASR products present what in 2D looks like a fibrillar morphology (Figure 3.6). In the more agglomerated areas, the product is densely packed and so the morphology cannot be clearly seen (Figure 3.6 (left)).
- All products are partly nanocrystalline as seen in Figure 3.7.

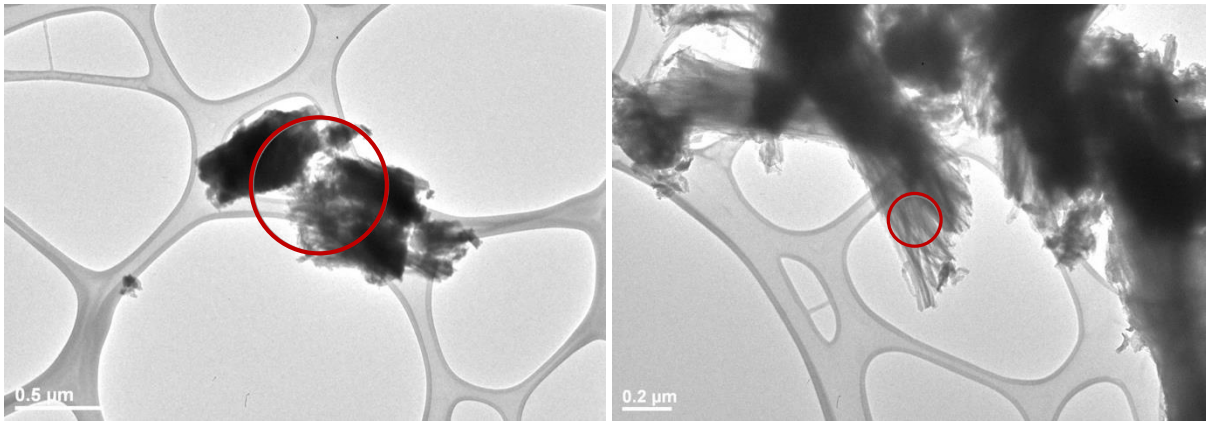


Figure 3.6: Globular (left) or fibrillar ASR-P1 (right) morphology of SKNC sample.

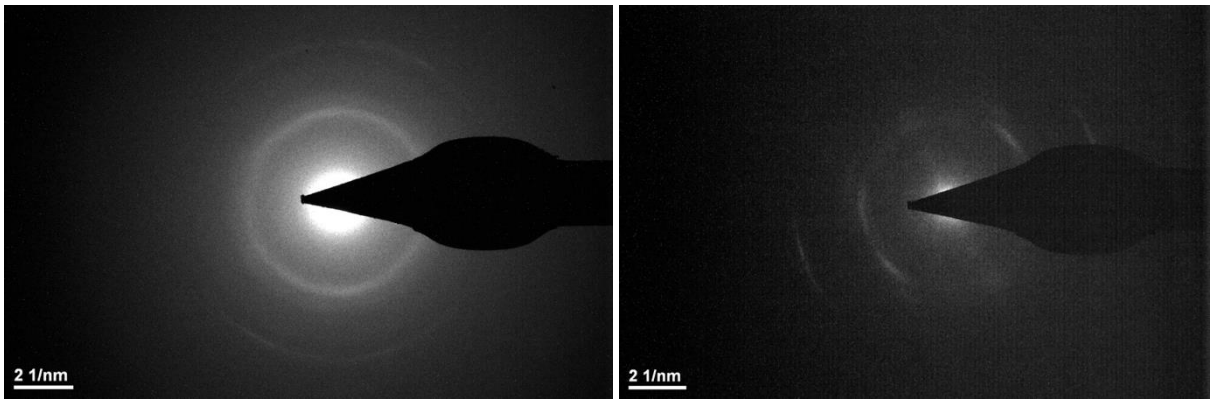


Figure 3.7: Diffraction patterns of “Figure 3.6 left” (left) and “Figure 3.6 right” red zones (right).

### 3.1.4 Field samples

Due to the low quantity of product present in these samples, the electron dose

In the case of the sample Dam, the product morphology is harder to assess compared to the synthetic one, indicating that the structure of these products are less ordered. In Figure 3.8 (left), L2 sample, no specific morphology appears, even though the product seems to be oriented parallel to the product/aggregate interface. The fissure were already present before beam exposure. For L1 (Figure 3.8 right) the platelet-like product morphology is visible, and also oriented parallelly to the product/aggregate interface. According to their diffraction pattern, both products were found to be amorphous.

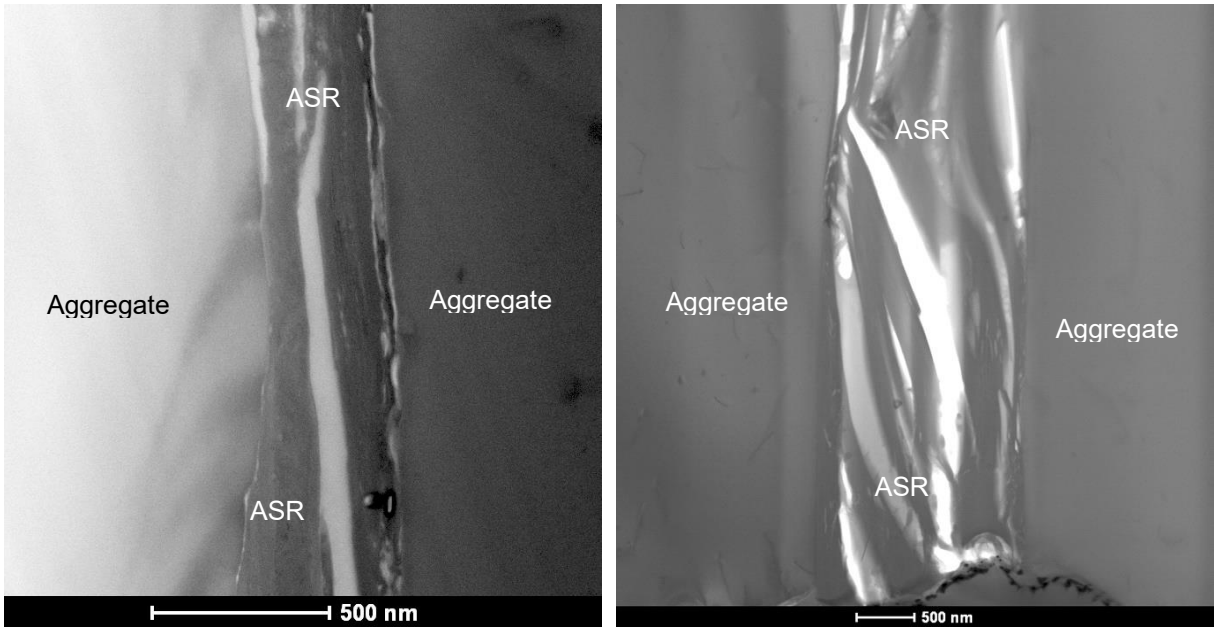


Figure 3.8: Dam L2 (left) and L1 (right) samples morphologies.

Two clear morphologies are visible in Brünig samples. In L1 Figure 3.10 (left), only platelet-like product was found, and in L2 Figure 3.10 (right) globular and platelet-like products were found.

Analysing the electron diffraction patterns with SAED, the products present in the Dam sample and the globular product in Brünig wall were found to be amorphous. However, SAED performed on the platelet-like product in Brünig sample L2 showed a diffraction pattern with two weak diffracting spots as seen in Figure 3.9.

The weakness of the diffraction spots indicates there is a low amount of ordered material in the analysed zone and it can be due to the following reasons:

- The product is only partially crystalline inducing very few diffracted electrons and thus a weak intensity.
- Even if used beam STEM operating conditions aimed at preserving the ASR products, it could have been damaged by electron beam, resulting in observation of amorphous product instead of crystalline one [15].

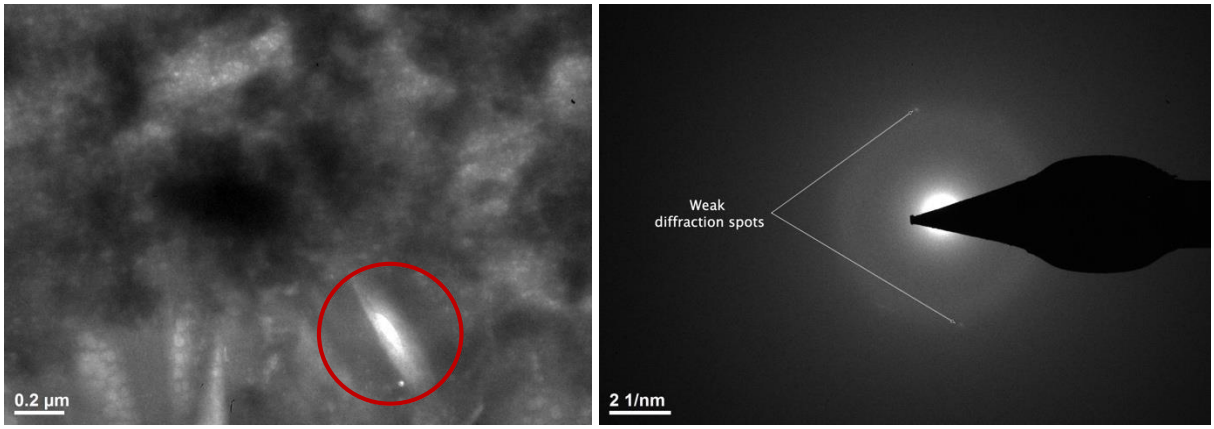


Figure 3.9: Brünig L2 amorphous (globular morphology) and crystalline (platelet-like morphology) (left) and diffraction pattern from the red zone showing a weak crystallinity (right).

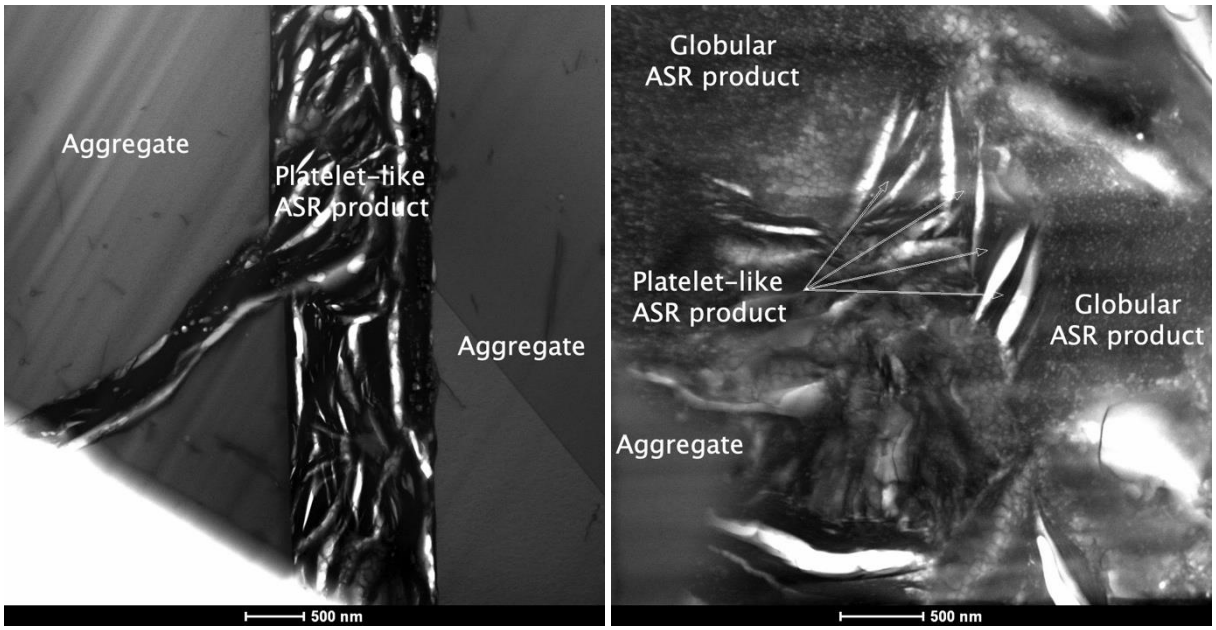


Figure 3.10: Brünig L1 showing platelet like morphology (but amorphous) (left) and Brünig L2 showing the intermixing of both globular and platelet-like morphologies (right).

## 3.2 Composition

The compositions presented in Table 3.1 are very similar between the different analyzed particles (L1 to L4) of each synthetic product, and also between the three synthetic products themselves. Only SKC seems to have a variation in the Ca/Si ratio, which again suggest a co-precipitation of C-S-H and ASR products in this sample [19]. L1 has a slightly higher calcium content compared to L2 and L3. If linked with the morphology and structure, L1 was the only particle to present a morphology in a platelet form and a crystalline structure, similar to SNC, in line with the fact that both Na-shlykovite and K-shlykovite have ideal alkali/Si ratio of 0.25. The other particles or agglomerates found were all having the rod-like appearance for ASR-P1 and fluffy appearance maybe for C-S-H (or broken ASR-P1 rods) with a microcrystalline structure, thus indicating calcium content might have a more significant role than alkali in the product formation. Both experimental studies and thermodynamic modelling showed that increasing the calcium content could destabilize the K-shlykovite to ASR-P1 and further to C-S-H [19].

The type of alkali and their proportion combination indicate to have an effect on the morphologies and structures as also reported in [16], since a difference in morphology and structure was observed between SNC and SNKC products, with no significant calcium but alkali content variation.

Table 3.1: Normalized composition of synthetic and field samples ASR product for different particles or lamellae.

| | | Si | Ca | K | Na | **Ca/Si** | **(K+Na)/Si** |
|---|---|---|---|---|---|---|---|
| | | at. % | at. % | at. % | at. % | at. % | at. % |
| SNC | L1 average | 64,06 | 17,02 | 0,09 | 18,83 | **0,27** | **0,30** |
| | L2 average | 67,25 | 15,74 | 0,06 | 16,95 | **0,23** | **0,25** |
| | L3 average | 65,67 | 15,70 | 0,07 | 18,56 | **0,24** | **0,28** |
| | L4 average | 64,23 | 15,09 | 0,03 | 20,65 | **0,23** | **0,32** |
| | | | | | | | |
| SKC | L1 average | 66,76 | 16,20 | 16,90 | 0,13 | **0,24** | **0,26** |
| | L2 average | 62,83 | 21,99 | 14,80 | 0,38 | **0,35** | **0,24** |
| | L3 average | 61,47 | 22,90 | 15,34 | 0,29 | **0,37** | **0,25** |
| | | | | | | | |
| SNKC | L1 average | 62,49 | 17,45 | 10,72 | 9,35 | **0,28** | **0,32** |
| | L2 average | 63,05 | 17,20 | 10,00 | 9,75 | **0,27** | **0,31** |
| | L3 average | 62,30 | 17,39 | 10,30 | 10,01 | **0,28** | **0,33** |
| | L4 average | 62,31 | 16,91 | 11,51 | 9,26 | **0,27** | **0,33** |
| | | | | | | | |
| Dam | L1 average | 65,95 | 17,88 | 14,94 | 0,43 | **0,27** | **0,25** |
| | L2 average | 63,26 | 21,38 | 9,12 | 7,26 | **0,34** | **0,24** |
| | | | | | | | |
| Brünig | L1 average | 60,38 | 15,06 | 19,20 | 5,35 | **0,25** | **0,42** |
| | L2 average AP | 43,50 | 25,43 | 26,32 | 4,76 | **0,59** | **0,77** |
| | L2 average Mix | 50,90 | 20,74 | 24,55 | 3,80 | **0,41** | **0,56** |
| | L2 average CP | 56,80 | 23,35 | 18,19 | 1,66 | **0,41** | **0,35** |

Globally, the normalized concentrations are very similar between all synthetic products, and also with the field samples Dam and Brünig L1.

Brünig L2 sample is different from L1, it is not part of the early stage products but it is rather some second stage product. Indeed, the ASR vein from where it was extracted is a few microns wide, and presence of amorphous and crystalline products could visually clearly be seen, based on the description from [14].

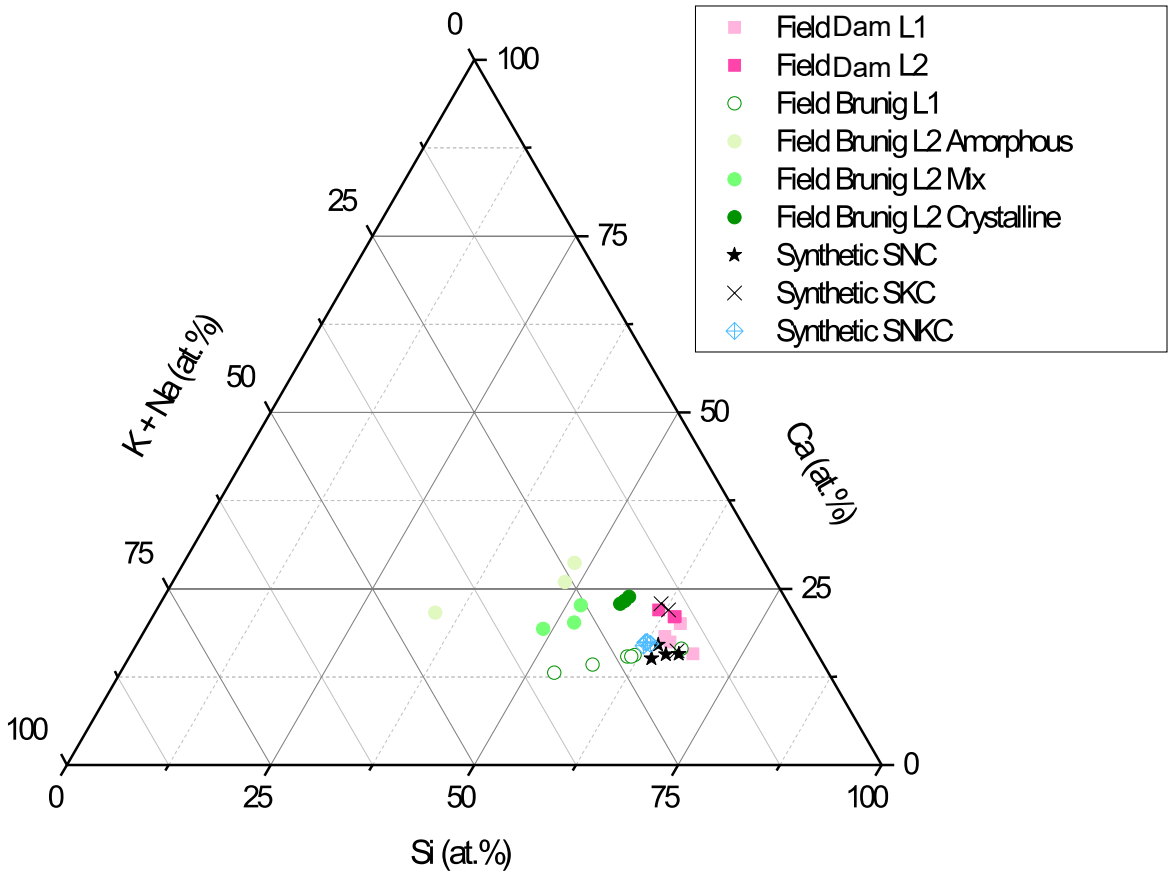


Figure 3.11: Ternary diagram presenting the normalized composition of ASR products from field and synthetic samples.

From the ternary diagram in Figure 3.11 presenting the above composition in a more visual way, the similarity in composition between all the products except Brünig L2 is obvious.

## 4. CONCLUSIONS

In this study, three synthesized ASR products with various alkali content as reported by [16] have been analysed by STEM to define their morphology, composition and structure. Two field products from different structures in Switzerland have also been analysed according to a new preparation method combining SEM, FIB and STEM described in [15]. The samples have been compared between each other and the following conclusions can be drawn from this preliminary study:

- ASR products are present in two very distinct morphologies: a platey and a fibrillar/globular morphology in both synthetic and field samples.
- The morphology is influenced by the calcium content and the initial K/Na molar ratios as seen in the synthetic samples.
- In synthetic samples, the structure is linked to the morphology: platey products are crystalline corresponding to K- or Na-shlykovite, and fibrillar/globular products are nanocrystalline (due to fibrils size) corresponding to ASR-P1 and/or eventually C-S-H.
- In field samples, some platey products are weakly crystalline whereas the globular products are amorphous. Due to the low amount of product, crystallinity is difficult to assess.
- Synthetic and some field samples are quite similar in terms of morphology and overall composition, but more samples from the field have to be analysed to validate it.
- Composition of crystalline products is similar.

- Additional field samples are needed to have more representative results concerning the early-stage ASR products, especially for the crystal structure.

The next step in this project is to analyse products synthesized at a temperature of 40°C in addition to 80°C. Indeed, a possibly more comparable temperature to field conditions will bring more insights about ASR product formation.

## 5. ACKNOWLEDGEMENTS

The authors would like to thank the Swiss National Science Foundation (SNSF) for the financial support through grant CRSII5_171018. In addition, Dr. Z. Shi would like to thank the financial support from the European union's Horizon 2020 research and innovation program under the Marie Skłodowska-Curie grant agreement number 754364. The authors would also like to thank the people of the Centre of Microscopy (CIME) of EPFL for their technical and scientific help, especially Dr. Marco Cantoni.

## 6. REFERENCES

[1] Merz C., Hunkeler F., Griesser A. (2006) Schäden durch Alkali-Aggregat-Reaktion an Betonbauten in der Schweiz, ASTRA-Bericht AGB2001/471, Bern

[2] Merz C., Leemann A. (2012) Validierung der AAR-Prüfungen für Neubau und Instandsetzung, ASTRA-Bericht. AGB 2005/023 und AGB 2006/003, 2012. Bern.

[3] Chatterji, S. (1979). The Role of Ca(OH)2 in the Breakdown of Portland Cement Concrete due to Alkali-Silica Reaction. Cement and Concrete Research, 9(2), 185-188.

[4] Dent Glasser, L., & Kataoka, N. (1981). The chemistry of 'alkali-aggregate' reaction. Cement and Concrete Research, 11(1), 1-9.

[5] Helmuth, R., Stark, D., Diamond, S., & Moranville-Regourd, M. (1993). Alkali-silica reactivity: an overview of research. Contract, 100, 202.

[6] Brouxel, M. (1993). The alkali-aggregate reaction rim: Na2O, SiO2, K2O and CaO chemical distribution. Cement and Concrete Research, 23(2), 309-320.

[7] Thaulow N, Jakobsen UH, Clark B (1996) Composition of alkali silica gel and ettringite in concrete railroad ties: SEM-EDX and X-ray diffraction analyses. Cem Concr Res 26(2):309-318. https://doi.org/10.1016/0008-8846(95)00219-7

[8] Marfil, S. A., & Maiza, P. J. (2001). Deteriorated pavements due to the alkali–silica reaction: a petrographic study of three cases in Argentina. Cement and Concrete Research, 31(7), 1017-1021.

[9] Kawamura, M., & Iwahori, K. (2004). ASR gel composition and expansive pressure in mortars under restraint. Cement and concrete composites, 26(1), 47-56.

[10] Fernandes I (2009) Composition of alkali-silica reaction products at different locations within concrete structures. Mater Charact 60(7): 655-668. https://doi.org/10.1016/j.matchar.2009.01.011

[11] Katayama T, (2012) ASR gels and their crystalline phases in concrete - universal products in alkali-silica, alkali-silicate and alkali-carbonate reactions. In Proceedings of the 14th International Conference on Alkali Aggregate Reactions (ICAAR), Austin, Texas, pp. 12.

[12] Leemann A, Lura P (2013) E-modulus of the alkali–silica-reaction product determined by micro-indentation. Constr Build Mater 44:221-227. https://doi.org/10.1016/j.conbuildmat.2013.03.018

[13] Leemann A, Merz C (2013) An attempt to validate the ultra-accelerated microbar and the concrete performance test with the degree of AAR-induced damage observed in concrete structures. Cem Concr Res 49:29-37. https://doi.org/10.1016/j.cemconres.2013.03.014

[14] Leemann, A., Katayama, T., Fernandes, I., Broekmans, M.A. (2016). Types of alkali–aggregate reactions and the products formed. Proc. Inst. Civ. Eng. Constr. Mater., 169, pp. 128-135

[15] Boehm-Courjault E., Barbotin S., Leemann A., Scrivener K. (2020) Microstructure, crystallinity and composition of alkali-silica reaction products in concrete determined by transmission electron microscopy, Cement and Concrete Research, Volume 130. https://doi.org/10.1016/j.cemconres.2020.105988

[16] Shi Z., Geng G., Leemann A., & Lothenbach B. (2019). Synthesis, characterization, and water uptake property of alkali-silica reaction products. Cement and Concrete Research, 121, 58-71.

[17] Shi, Z., & Lothenbach, B. (2020). The combined effect of potassium, sodium and calcium on the formation of alkali-silica reaction products. Cement and Concrete Research, 127, 105914.

[18] Roessler C., Stark J., Steiniger F., Tichelaar W. (2006) Limited-dose electron microscopy reveals the crystallinity of fibrous C-S-H phases, J. Am. Ceram. Soc., 89 (2), pp. 627-632.

[19] Shi, Z., & Lothenbach, B. (2019). The role of calcium on the formation of alkali-silica reaction products. Cement and Concrete Research, 126, 105898.